A Low-Switching-Frequency Flux Observer and Torque Model of Deadbeat–Direct Torque and Flux Control on Induction Machine Drives

Yukai Wang, *Student Member, IEEE*, Shunsuke Tobayashi, and Robert D. Lorenz, *Fellow, IEEE*

***Abstract*—This paper presents a digital implementation of deadbeat–direct torque and flux control (DB-DTFC) for induction machines at low switching frequencies (SFs). For high SFs, existing discrete-time flux observers and Volt–second-based inverse torque models used for DB-DTFC achieve acceptable flux estimation accuracy and fast torque response. However, the flux estimate is less accurate when the SF is reduced and the DB-DTFC performance degrades. This paper develops a more suitable flux observer and Volt–second-based inverse torque model that minimizes flux estimation error and improves torque control for DB-DTFC. Simulation and experimental results are provided to evaluate the performance of the proposed observer and torque model at very low SFs. Consequently, digital implementation of low-SF DB-DTFC on high-power induction machines is feasible.**

***Index Terms*—Deadbeat–direct torque and flux control (DB-DTFC), flux observer, low-switching-frequency (SF) operation.**

NOMENCLATURE

$(\,)^s$	Stationary reference frame.
$(\,)^r$	Rotor reference frame.
$(\hat{})$	Estimation quantity.
$(\,)^*$	Reference quantity.
$\dot{(\,)}$	Time derivative operator.
$(\,)_s$	Quantity on the stator side.
$(\,)_r$	Quantity on the rotor side.
$(\,)_{qdx}$	Complex vector quantity.
(k)	Quantity at the kth sampling time.
(s)	Quantity in the Laplace domain.
s	Laplace operator.
v_{qds}	Stator voltage complex vector.
i_{qds}	Stator current complex vector.
i_{qdr}	Rotor current complex vector.
λ_{qds}	Stator flux linkage complex vector.
i_{qdr}	Rotor flux linkage complex vector.
R_s	Stator resistance.
R_r	Rotor resistance.
L_m	Magnetizing inductance.
L_{ls}	Stator leakage inductance.
L_{lr}	Rotor leakage inductance.
$\sigma = 1 - (L_m L_m / L_s L_r)$	Total leakage factor.
$\tau_r = R_r / L_r$	Rotor time constant.
ω_r	Electrical angular velocity of rotor.
$\omega_{br} = (R_r / L_r) - j\omega_r$	Rotor break frequency.
T_e	Electromagnetic torque.
T_s	Sampling time.

Manuscript received March 8, 2014; revised May 28, 2014 and September 5, 2014; accepted September 30, 2014. Date of publication October 29, 2014; date of current version May 15, 2015. Paper 2014-IDC-0131.R2, presented at the 2013 IEEE Energy Conversion Congress and Exposition, Denver, CO, USA, September 16–20, and approved for publication in the IEEE TRANSACTIONS ON INDUSTRY APPLICATIONS by the Industrial Drives Committee of the IEEE Industry Applications Society. This work was supported by Toshiba Mitsubishi–Electric Industrial Systems Corporation, Fuchu, Japan.

Y. Wang and R. D. Lorenz are with the Wisconsin Electric Machines and Power Electronics Consortium, University of Wisconsin–Madison, Madison, WI 53706 USA (e-mail: ywang289@wisc.edu; lorenz@engr.wisc.edu).

S. Tobayashi is with Toshiba Mitsubishi–Electric Industrial Systems Corporation, Fuchu 104-0031, Japan (e-mail: TOBAYASHI.shunsuke@tmeic.co.jp).

Color versions of one or more of the figures in this paper are available online at http://ieeexplore.ieee.org.

Digital Object Identifier 10.1109/TIA.2014.2365628

I. INTRODUCTION

DEADBEAT–DIRECT torque and flux control (DB-DTFC) is a promising alternative to indirect field-oriented control (IFOC) for induction machines [1]–[5]. Unlike IFOC, which relies on properties of the current regulator [6], DB-DTFC manipulates the inverter Volt–second vectors directly over the entire operating space using a single control law [3]. In addition to the air-gap torque, stator flux linkage is used as a simultaneous control variable to dynamically manipulate loss, which is not a straightforward process to achieve via IFOC. Compared to traditional direct torque control using hysteretic comparators [7], [8], the switching period of DB-DTFC is fixed, which offers the potential to integrate advanced ac machine control techniques such as self-sensing.

The performance of DB-DTFC depends on a properly formed discrete-time flux observer to estimate flux and an accurate inverse torque model to compute the Volt–second solution for each switching interval. The development and implementation of flux observers have been widely explored in literature, mostly using continuous-time-domain analysis and transforming into discrete-time domain with first-order approximation (also referred to as Euler approximation) [9]–[15]. The existed DB-DTFC drives [1]–[3] utilize flux observer topology illustrated in [9] and follow digital implementation approaches provided in [10]. By combining the current model and the voltage model of induction machine, reliable estimation accuracy and insensitivity to parameters are demonstrated. The flux linkage estimates are then used to compute the deadbeat Volt–second control law based on the induction machine torque model. A graphical Volt–second solution can be used to document the simplicity of the control law to achieve the commanded torque

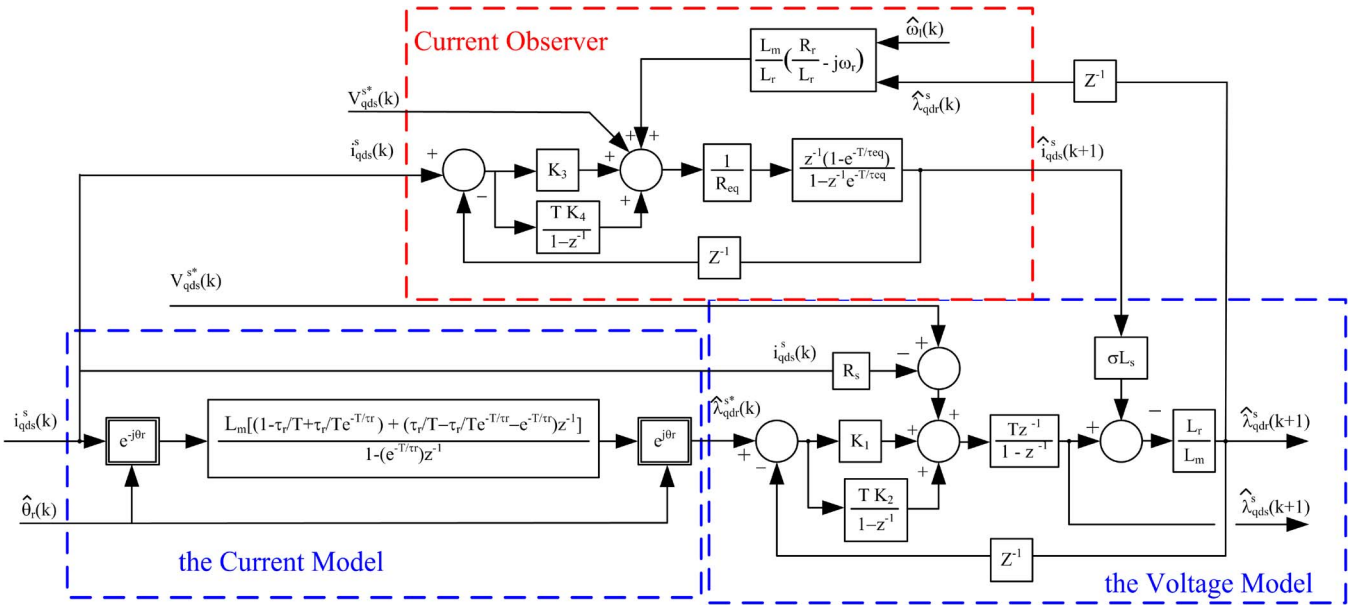

Fig. 1. State block diagram for the high-SF flux observer system [10].

and simultaneously have a separate degree of freedom for loss manipulation [3].

Although the accuracy of this flux observer and Volt–second-based inverse torque model has been evaluated at high switching frequencies (SFs) (e.g., 10 kHz), DB-DTFC on an induction machine at low SFs has not yet been investigated. For high-power induction machine drives, however, switching losses force the use of low SFs. The approximations embedded in the flux observer structure and torque models might not be valid for low-SF operation.

In the literature, developments of low-SF flux observers and induction models have been given in [16]–[19], using various discretization algorithms. The proposed method in [16], using exact discretization on the time-varying matrix, demonstrates significant improvements over the Euler approximation at low sampling frequencies. The solution is developed in the synchronous reference frame and evaluated on a V/F induction motor drive by simulation. The solutions provided in [17] require no assumption of constant voltage over each discrete step but need input voltage known in advance (e.g., sinusoidal voltage). Thus, it is not suitable for fast dynamic applications fed by a pulsewidth-modulation (PWM) voltage source. Pole mitigation analysis has been provided in [18] and [19], and an unstable region due to use of first-order approximation has been explicitly documented. Computationally optimized solutions are provided and compared with first- and second-order Euler approximations.

This paper presents a cross-coupled discrete-time system modeling methodology for DB-DTFC drive operating at low SFs. The methodology follows an exact discretization approach, with the assumption of constant speed over one switching period. Using this methodology, an enhanced flux observer and an enhanced torque inverse model are developed as solution for a DB-DTFC drive operating at low SFs, and their performance is compared with the existing DB-DTFC solutions with high-SF approximations [1], [2], [10]. The flux observer is modified to provide accurate estimates of stator and rotor flux linkages without the usual high-SF approximations and also be suitable for torque estimation at low SFs. A low-SF Volt–second-based inverse torque model of the induction machine is developed to achieve the desired deadbeat control of air-gap torque response. The proposed low-SF DB-DTFC models are evaluated in simulation and experiments in Sections IV and V, respectively. Possibility to integrate low-SF DB-DTFC on high-power machines is further explored in Section VI.

It may be necessary to clarify the terms of "high-/low-SF model" and the use of "Euler approximation" and "exact discretization." Indeed, the existing high-SF DB-DTFC model employs models based on the Euler approximation, while the proposed low-SF model follows an exact discretization methodology. From the standpoint of motor drives, however, the use of either model primarily depends on the system power rating and the SF. To be more application oriented, the terms "high-/low-SF models" are used in the rest of this paper.

II. Low-SF Flux Observer

A. High-SF Flux Observer

Digital implementation of a stator and rotor flux observer has been proposed in [10], by combining the current model and the voltage model. A state block diagram of the closed-loop observer system is shown in Fig. 1. It has been demonstrated to possess good estimation accuracy and performance when integrated with DB-DTFC at relatively high SFs (e.g., 10 kHz).

The sensitivity to low SFs should be investigated on both the current model and the voltage model. For the current model, the measured current is used to estimate rotor flux based on the relationship shown in (1), where the rotor reference frame is used to eliminate the rotor speed dependence. For digital implementation, a ramp interface for stator current is assumed because the stator current in the rotor reference frame can be seen as a sinusoidal waveform at the slip frequency. Even at

low SFs, this assumption is still acceptable because of the slow slip frequency. Therefore, this current model is still valid. The difference equation for implementation is based on (2)

$$\dot{\lambda}^r_{qdr} = \frac{R_r}{L_r} L_m i^r_{qds} - \frac{R_r}{L_r}\lambda^r_{qdr} \tag{1}$$

$$\begin{aligned}\lambda^r_{qdr}(k) = &\left(1 - \frac{\tau_r}{T_s} + \frac{\tau_r}{T_s} e^{-T_s/\tau_r}\right) L_m i^r_{qds}(k) \\ &+ \left(\frac{\tau_r}{T_s} - \left(\frac{\tau_r}{T_s} + 1\right) e^{-T} s/\tau_r\right) L_m i^r_{qds}(k-1) \\ &+ e^{-T} s/\tau_r \lambda^r_{qdr}(k-1).\end{aligned} \tag{2}$$

The voltage model in this flux observer model becomes problematic at low SFs. In the continuous-time domain, stator voltage and current are used to estimate stator flux linkage based on the relationship shown in (3). For digital implementation, the average rate of change of stator flux linkage approximates the flux derivative as shown in (4), which is less accurate when switching slowly. Another unacceptable approximation at low SFs is the assumption that the stator current is constant during the sample interval. Comparing (4) to (3), stator flux and current are treated as two independent states, and the cross-coupling between them is ignored

$$\dot{\lambda}^s_{qds} = v^s_{qds} - R_s i^s_{qds} \tag{3}$$

$$\frac{\lambda^s_{qds}(k+1) - \lambda^s_{qds}(k)}{T_s} = v^s_{qds}(k) - R_s i^s_{qds}(k). \tag{4}$$

B. Methodology for Discrete-Time Modeling

Before discussions about low-SF flux observers and torque models, a principle methodology for modeling a discrete-time cross-coupled system is generalized and proposed as follows.

Step I) Prepare continuous-time-domain differential equations of relevant state variables.

Step II) Form the Laplace transform of the differential equations, including the effects of initial conditions.

Step III) Cross-solve the Laplace-transformed equations for each state as needed. Only initial conditions from cross-coupled states and inputs should remain.

Step IV) Substitute the latched model for the manipulated inputs in the equations obtained in Step III).

Step V) Find the continuous-time step response based on inverse Laplace transformation.

Step VI) Find the cross-coupled response at the next sampling instant, and generalize into sampled time domain.

Both low-SF flux observer and Volt–second-based torque model for induction machine have been developed strictly following the aforementioned procedure. The discrete-time modeling methodology is also applicable for other systems, like interior permanent-magnet synchronous machines [20].

C. Low-SF Flux Observer

Following the modeling methodology, a low-SF flux observer is derived in this section without fast high-SF approximations.

In terms of fundamental continuous-time-domain differential equations (Step I), rotor flux differential (5) and relationships between flux linkages (6) and (7) have been used in addition to stator flux differential (3) used for the high-SF flux observer

$$\dot{\lambda}^s_{qdr} = -R_r i^s_{qdr} + j\omega_r \lambda^s_{qdr} \tag{5}$$

$$\lambda^s_{qds} = L_s i^s_{qds} + L_m i^s_{qdr} \tag{6}$$

$$\lambda^s_{qdr} = L_m i^s_{qds} + L_r i^s_{qdr}. \tag{7}$$

By cross-solving (5)–(7), the following equation is obtained with the states of stator flux linkage and stator current remaining only:

$$\dot{\lambda}^s_{qds} + \omega_{br}\lambda^s_{qds} = \sigma L_s \dot{i}^s_{qds} + L_s\left(\frac{R_r}{L_r} - j\sigma\omega_r\right) i^s_{qds}. \tag{8}$$

By assuming that the change of rotor speed over one switching period is negligible, the Laplace transform is applied to (3) and (8) as Step II). It results in the Laplace-transformed differential equations, as shown in (9) and (10), for stator flux and stator current, respectively. It is noted that the initial conditions should be included in the transformation

$$s\lambda^s_{qds}(s) = v^s_{qds}(s) - R_s i^s_{qds}(s) + \lambda^s_{qds}(t=0) \tag{9}$$

$$\begin{aligned}&(s+\omega_{br})\lambda^s_{qds}(s) - \lambda^s_{qds}(t=0) \\ &\quad = \left(\sigma L_s s + L_s\left(\frac{R_r}{L_r} - j\omega_r\sigma\right)\right) i^s_{qds}(s) - \sigma L_s i^s_{qds}(t=0).\end{aligned} \tag{10}$$

For an induction machine driven by a voltage source inverter, the machine terminal voltage is the true manipulated input. The latched model (11) is suitable to describe its characteristic of step input

$$v_{qds}(s) = \frac{v_{qds}(t=0)}{s}. \tag{11}$$

By cross-solving the Laplace-transformed differential (9) and (10) for stator flux linkage as Step III) and substituting the manipulated input variable by the latched model (11) as Step IV, the state of stator flux linkage in s-domain is described only by the manipulated input and initial conditions in (12). The eigenvalues in (12) are identified as τ_1 and τ_2 in (13)

$$\begin{aligned}\lambda^s_{qds}(s) = &\frac{s + \frac{R_r}{L_r\sigma} - j\omega_r}{s(s+\tau_1)(s+\tau_2)} v^s_{qds}(t=0) \\ &+ \frac{s + \frac{R_r}{L_r\sigma} + \frac{R_s}{L_s\sigma} - j\omega_r}{(s+\tau_1)(s+\tau_2)} \lambda^s_{qds}(t=0) \\ &- \frac{R_s}{(s+\tau_1)} i^s_{qds}(t=0)\end{aligned} \tag{12}$$

$$(s+\tau_1)(s+\tau_2) = s^2 + \left(\frac{R_r}{L_r\sigma} + \frac{R_s}{L_s\sigma} - j\omega_r\right) s + \frac{R_s\omega_{br}}{L_s\sigma}. \tag{13}$$

To find out the continuous-time step response solution, the Laplace inverse transform is applied on (12) as Step V). The result is shown in the following, which indicates the response to a step input in the time domain with given initial conditions:

$$\lambda^s_{qds}(T_s) = F_v v^s_{qds}(t=0) + F_\lambda \lambda^s_{qds}(t=0) + F_i i^s_{qds}(t=0) \tag{14}$$

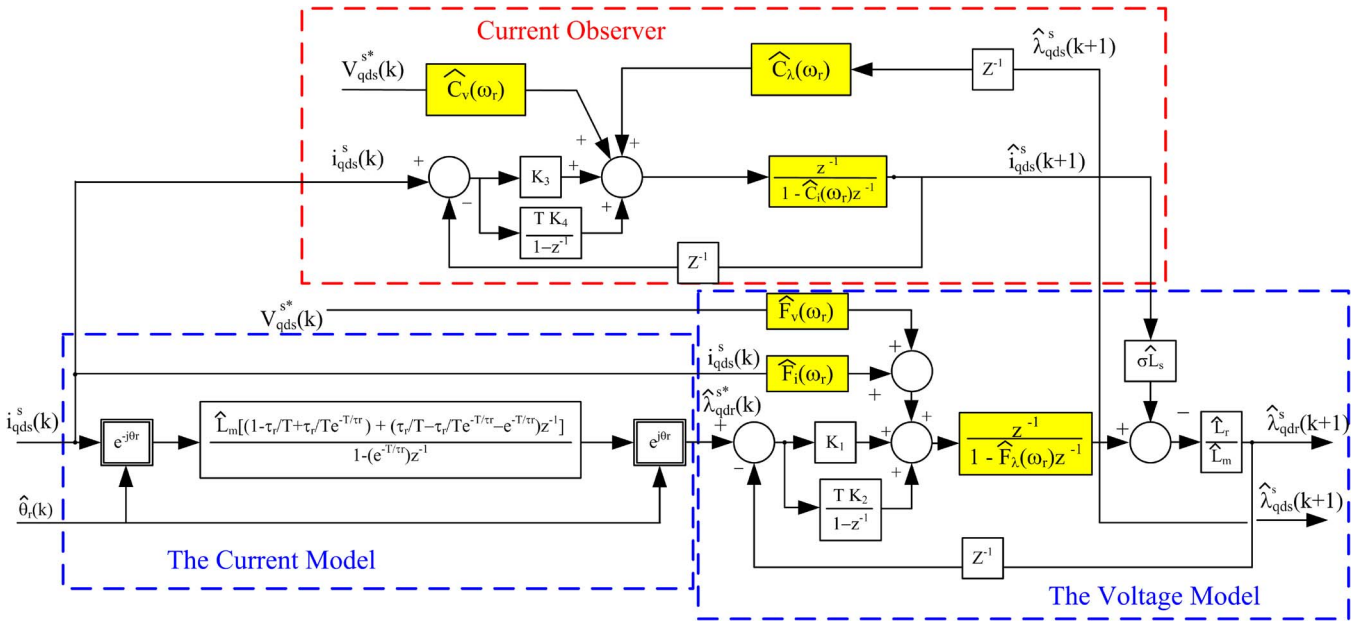

Fig. 2. State block diagram for the proposed low-SF flux observer system.

where

$$F_v = \frac{\frac{R_r}{\sigma L_r} - j\omega_r}{\tau_1\tau_2} + \frac{\frac{R_r}{\sigma L_r} - j\omega_r - \tau_1}{\tau_1(\tau_1-\tau_2)}e^{-\tau_1 T_s} - \frac{\frac{R_r}{\sigma L_r} - j\omega_r - \tau_2}{\tau_2(\tau_1-\tau_2)}e^{-\tau_2 T_s}$$

$$F_\lambda = \frac{-\tau_2}{\tau_1-\tau_2}e^{-\tau_1 T_s} + \frac{\tau_1}{\tau_1-\tau_2}e^{-\tau_2 T_s}$$

$$F_i = \frac{R_s}{\tau_1-\tau_2}e^{-\tau_1 T_s} - \frac{R_s}{\tau_1-\tau_2}e^{-\tau_2 T_s}.$$

In the sampled time domain, (14) can be generalized to an arbitrary time kT as the final step, and the final recursive cross-coupled state equation for stator flux linkage is obtained as

$$\lambda^s_{qds}(k+1) = F_v v^s_{qds}(k) + F_\lambda \lambda^s_{qds}(k) + F_i i^s_{qds}(k). \quad (15)$$

The same methodology is followed by cross-solving (9) and (10) to achieve the recursive cross-coupled state equations for stator current. The Laplace inverse transform is applied, which yields the response in continuous-time domain. It can be then generalized to the sampled time domain as (16). This effort improves the current observer, which provides the current estimates at the next switching instant that do not have a lagging property [10]

$$i^s_{qds}(k+1) = C_v v^s_{qds}(k) + C_\lambda \lambda^s_{qds}(k) + C_i i^s_{qds}(k). \quad (16)$$

The recursive equations for stator flux linkage (15) and current (16) can be used to modify the flux observer model shown in Fig. 1. A corresponding state block diagram of the proposed low-SF flux observer is shown in Fig. 2.

D. Flux Observer Comparison

By simple term arrangement of (4), the recursive equation for the high-SF flux observer is obtained as

$$\lambda^s_{qds}(k+1) = T_s v^s_{qds}(k) + \lambda^s_{qds}(k) - R_s T_s i^s_{qds}(k). \quad (17)$$

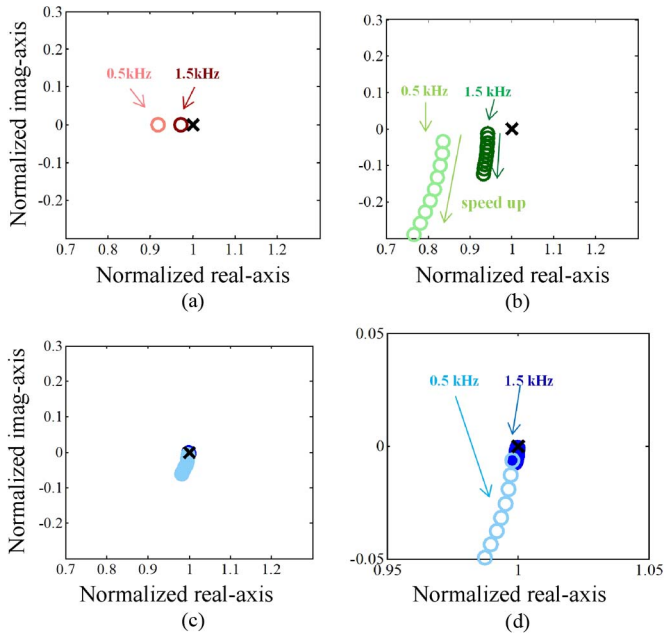

Fig. 3. Coefficient comparisons of the proposed flux observer at 1.5 and 0.5 kHz with the existing flux observer. Coefficient comparison for (a) $V_{qds}(k)$, (b) $I_{qds}(k)$, (c) $\lambda_{qds}(k)$, and (d) a zoomed-in view of (c).

It is indicated in recursive (15) and (17) that the discrete-time state variables and the manipulated input are identical for the low- and the high-SF flux observer. However, the coefficients for the two models are different. For a fair comparison, the time-invariant coefficients in the high-SF flux observer (17) have been used as base values and placed in the center in Fig. 3. On the other hand, corresponding coefficients used in the proposed low-SF flux observer are varying at different operating speeds. In particular, the coefficients at SFs of 1.5 and 0.5 kHz are calculated as a function of operating speed and normalized by the their counterparts in the high-SF flux observer and shown in Fig. 3.

The discrepancy of the proposed low-SF flux observer has been clearly demonstrated in Fig. 3. Since complex variables have been used in previous derivation, deviations on real axis indicate the magnitude difference, while deviations on image axis represent unmodeled cross-coupling effects due to the use of high-SF approximations. At a relatively high SF of 1.5 kHz, the coefficients in the proposed flux observer are fairly close to its counterparts in the existing flux observer. However, significant differences emerge when the SF is reduced to 0.5 kHz, from a perspective of magnitude and/or unmodeled cross-coupling effects. It is safe to conclude that the proposed low-SF flux observer is a more accurate form and applicable to both high and low SFs for which the coefficients are calculated.

III. Low-SF Torque Inverse Model

A. High-SF Torque Inverse Model

It was proposed in [2] that the induction machine inverse model can be used to create a deadbeat control law. The fundamental expression of air-gap torque equation is given in terms of flux linkages as (18). The torque differential equation (19) is obtained by taking the derivative of (18) and substituting the stator and rotor flux differentials (3) and (5)

$$T_e = \frac{3P}{4}\frac{L_m}{\sigma L_s L_r}(\lambda_{qs}\lambda_{dr} - \lambda_{ds}\lambda_{qr}) \tag{18}$$

$$\dot{T}_e = \frac{3P}{4}\frac{L_m}{\sigma L_s L_r}\left(v_{qs}\lambda_{dr} - v_{ds}\lambda_{qr} - \omega_r\left(\lambda_{qs}\lambda_{qr} + \lambda_{ds}\lambda_{dr}\right)\right) - \left(\frac{R_r L_s + R_s L_r}{\sigma L_s L_r}\right) T_e. \tag{19}$$

For digital implementation of DB-DTFC at high SFs, the average rate of change of torque can be used as an approximation for the torque derivative (20), to form the sampled-time-domain difference equation as (21). However, this assumption yields torque control error when the SF is reduced

$$\dot{T}_e = \frac{T_e(k+1) - T_e(k)}{T_s} \tag{20}$$

$$\begin{aligned} v_{qs}(k)T_s = {} & \frac{\lambda_{qr}(k)}{\lambda_{dr}(k)} v_{ds}(k)T_s \\ & + \frac{T_s\omega_r(k)}{\lambda_{dr}(k)}\left(\lambda_{qs}(k)\lambda_{qr}(k) + \lambda_{ds}(k)\lambda_{dr}(k)\right) \\ & + \frac{1}{\left(\frac{3P}{4}\frac{L_m}{\sigma L_s L_r}\right)\lambda_{dr}(k)} \\ & \times \left(\Delta T_e(k) + T_s\left(\frac{R_r L_s + R_s L_r}{\sigma L_s L_r}\right) T_e(k)\right). \end{aligned} \tag{21}$$

B. Low-SF Torque Inverse Model

An accurate Volt–second-based inverse torque model, particularly for low-SF operation, is derived in this section. The methodology used is following the one provided in Section II-B. Stator and rotor flux differential equations, as the fundamental relations employed, are presented in the following in a matrix form:

$$\begin{bmatrix} \dot{\lambda}^s_{qs} \\ \dot{\lambda}^s_{ds} \\ \dot{\lambda}^s_{qr} \\ \dot{\lambda}^s_{dr} \end{bmatrix} = \begin{bmatrix} -\frac{R_s}{\sigma L_s} & 0 & \frac{R_s L_m}{\sigma L_s L_r} & 0 \\ 0 & -\frac{R_s}{\sigma L_s} & 0 & \frac{R_s L_m}{\sigma L_s L_r} \\ \frac{R_r L_m}{\sigma L_s L_r} & 0 & -\frac{R_r}{\sigma L_r} & \omega_r \\ 0 & \frac{R_r L_m}{\sigma L_s L_r} & -\omega_r & -\frac{R_r}{\sigma L_r} \end{bmatrix} \begin{bmatrix} \lambda^s_{qs} \\ \lambda^s_{ds} \\ \lambda^s_{qr} \\ \lambda^s_{dr} \end{bmatrix} + \begin{bmatrix} 1 & 0 \\ 0 & 1 \\ 0 & 0 \\ 0 & 0 \end{bmatrix} \begin{bmatrix} v^s_{qs} \\ v^s_{ds} \end{bmatrix}. \tag{22}$$

Assuming that rotor speed changes over one switching period are negligible, the Laplace transform including the initial conditions is applied to flux differential (22). The resulted cross-coupled s-domain stator and rotor flux linkage differential equations are shown as follows, where the voltage states are the true manipulated inputs:

$$\begin{bmatrix} s\lambda^s_{qs}(\boldsymbol{s}) - \lambda^s_{qs}(t=0) \\ s\lambda^s_{ds}(\boldsymbol{s}) - \lambda^s_{ds}(t=0) \\ s\lambda^s_{qr}(\boldsymbol{s}) - \lambda^s_{qr}(t=0) \\ s\lambda^s_{dr}(\boldsymbol{s}) - \lambda^s_{dr}(t=0) \end{bmatrix} = \begin{bmatrix} -\frac{R_s}{\sigma L_s} & 0 & \frac{R_s L_m}{\sigma L_s L_r} & 0 \\ 0 & -\frac{R_s}{\sigma L_s} & 0 & \frac{R_s L_m}{\sigma L_s L_r} \\ \frac{R_r L_m}{\sigma L_s L_r} & 0 & -\frac{R_r}{\sigma L_r} & \omega_r \\ 0 & \frac{R_r L_m}{\sigma L_s L_r} & -\omega_r & -\frac{R_r}{\sigma L_r} \end{bmatrix} \times \begin{bmatrix} \lambda^s_{qs}(\boldsymbol{s}) \\ \lambda^s_{ds}(\boldsymbol{s}) \\ \lambda^s_{qr}(\boldsymbol{s}) \\ \lambda^s_{dr}(\boldsymbol{s}) \end{bmatrix} + \begin{bmatrix} 1 & 0 \\ 0 & 1 \\ 0 & 0 \\ 0 & 0 \end{bmatrix} \begin{bmatrix} v^s_{qs}(\boldsymbol{s}) \\ v^s_{ds}(\boldsymbol{s}) \end{bmatrix}. \tag{23}$$

As stated in Section II, the manipulated inputs can be modeled as a latched interface by (11). The states of stator and rotor flux linkages, in the s-domain, can be cross-solved as (24). Only the manipulated inputs [e.g., $v_{qds}(t=0)$] and initial conditions [e.g., $\lambda_{qds}(t=0)$ and $\lambda_{qdr}(t=0)$] remain

$$\begin{bmatrix} \lambda^s_{qs}(\boldsymbol{s}) \\ \lambda^s_{ds}(\boldsymbol{s}) \\ \lambda^s_{qr}(\boldsymbol{s}) \\ \lambda^s_{dr}(\boldsymbol{s}) \end{bmatrix} = \begin{bmatrix} \boldsymbol{s} + \frac{R_s}{\sigma L_s} & 0 & -\frac{R_s L_m}{\sigma L_s L_r} & 0 \\ 0 & \boldsymbol{s} + \frac{R_s}{\sigma L_s} & 0 & -\frac{R_s L_m}{\sigma L_s L_r} \\ -\frac{R_r L_m}{\sigma L_s L_r} & 0 & \boldsymbol{s} + \frac{R_r}{\sigma L_r} & -\omega_r \\ 0 & -\frac{R_r L_m}{\sigma L_s L_r} & \omega_r & \boldsymbol{s} + \frac{R_r}{\sigma L_r} \end{bmatrix}^{-1} \times \begin{bmatrix} \frac{1}{s} & 0 & 1 & 0 & 0 & 0 \\ 0 & \frac{1}{s} & 0 & 1 & 0 & 0 \\ 0 & 0 & 0 & 0 & 1 & 0 \\ 0 & 0 & 0 & 0 & 0 & 1 \end{bmatrix} \begin{bmatrix} v^s_{qs}(t=0) \\ v^s_{ds}(t=0) \\ \lambda^s_{qs}(t=0) \\ \lambda^s_{ds}(t=0) \\ \lambda^s_{qr}(t=0) \\ \lambda^s_{dr}(t=0) \end{bmatrix}. \tag{24}$$

The Laplace inverse transform is applied on all four s-domain flux differential equations in (24) to achieve continuous-time step response solutions. After generalizing to an arbitrary time kT, recursive equations for stator and rotor flux linkages are obtained and expressed in a matrix format

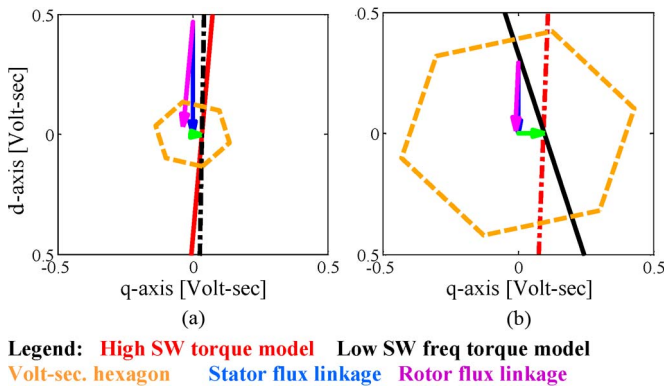

Fig. 4. Inverse torque model comparisons using the DB-DTFC graphical solution. Switching at (a) 1.5 and (b) 0.5 kHz.

in (25). Each element, in the coefficient matrix (e.g., B_{ij}), is obtained from the Laplace inverse transformation

$$\begin{bmatrix} \lambda^s_{qs}(\boldsymbol{k}+\mathbf{1}) \\ \lambda^s_{ds}(\boldsymbol{k}+\mathbf{1}) \\ \lambda^s_{qr}(\boldsymbol{k}+\mathbf{1}) \\ \lambda^s_{dr}(\boldsymbol{k}+\mathbf{1}) \end{bmatrix} = \begin{bmatrix} B_{11} & B_{12} & B_{13} & B_{14} & B_{15} & B_{16} \\ B_{21} & B_{22} & B_{23} & B_{24} & B_{25} & B_{26} \\ B_{31} & B_{32} & B_{33} & B_{34} & B_{35} & B_{36} \\ B_{41} & B_{42} & B_{43} & B_{44} & B_{45} & B_{46} \end{bmatrix} \times \begin{bmatrix} v^s_{qs}(k) \\ v^s_{ds}(k) \\ \lambda^s_{qs}(k) \\ \lambda^s_{ds}(k) \\ \lambda^s_{qr}(k) \\ \lambda^s_{dr}(k) \end{bmatrix}. \quad (25)$$

The well-known induction machine torque equation shown in (18) can be expressed in the sampled time domain as

$$T_e(k+1) = \frac{3P}{4}\frac{L_m}{\sigma L_s L_r}\left(\lambda^s_{qs}(k+1)\lambda^s_{dr}(k+1) - \lambda^s_{ds}(k+1)\lambda^s_{qr}(k+1)\right). \quad (26)$$

The flux linkages at the next switching instant [e.g., $\lambda_{qds}(k+1)$] can be substituted by the recursive equations shown in (25). In addition, the term $T_e(k+1)$ in (26) represents the desired air-gap torque at the next switching instant, which is theoretically the torque command at the current time $T^*_e(k)$. By rearrangement of (26), a torque inverse model is obtained in (27), which is similar to (21). Coefficients (i.e., m_1, m_2, and m_3) are functions of speed, SF, and machine parameters

$$V^s_{qs}(k)T_s = -\frac{m_1(k)}{m_2(k)}V^s_{ds}(k)T_s + \frac{T^*_e(k) - m_3(k)}{m_2(k)}T_s. \quad (27)$$

The solution obtained in (27) demonstrates a unique Volt–second-based torque model to produce desired torque and stator flux magnitude simultaneously. Compared to (21), this torque inverse model does not contain fast switching assumption (20) and should remain accurate at any SF that the coefficients are calculated for.

Fig. 4 provides the comparison of the two torque inverse models using the DB-DTFC graphical solution. For each switching instant, the Volt–second solution is computed so that both air-gap torque and stator flux magnitude commands can be achieved. The difference between the two solutions is shown more significantly in Fig. 4(b), where the SF is as low as 0.5 kHz. Inevitable torque control error is expected when the high-SF torque model is used for low-SF operation.

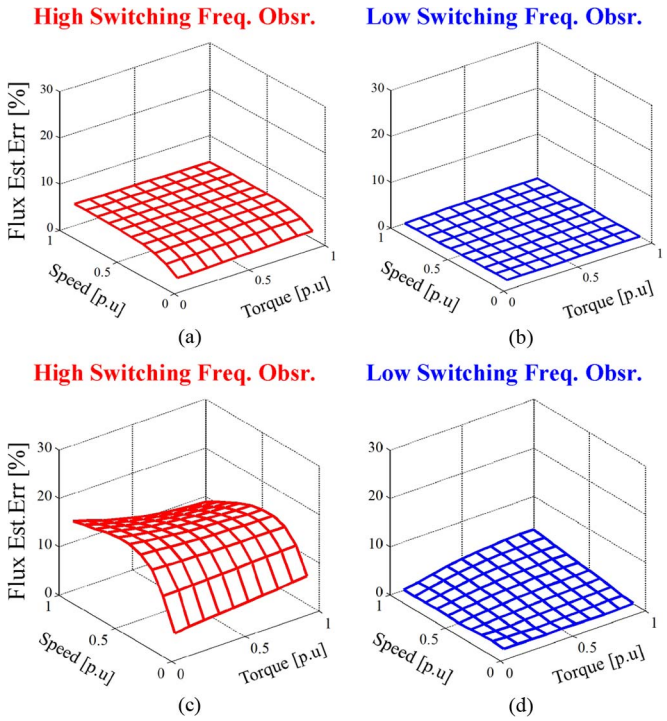

Fig. 5. Flux estimation errors in simulation using the high or low SF flux observer at rated flux switching at [(a) and (b)] 1.5 and [(c) and (d)] 0.5 kHz.

IV. Simulation Results

A low-SF flux observer and a Volt–second-based torque inverse model are proposed in Sections II and III, respectively, to improve DB-DTFC performance at low SFs. The main foci of this section are to evaluate the effectiveness of the low-SF DB-DTFC and to compare it to its high-SF counterpart with the aforementioned approximations. Note that DB-DTFC performance relies on accurate estimates of flux linkages from the flux observer and a proper torque model to solve for the Volt–second vectors for each switching interval. In simulation, an induction machine with key parameters provided in Appendix I is used.

A. Flux Observer Evaluation

In order to give a fair comparison of the proposed low-SF flux observer to the existing one with high-SF approximations, the following concerns are provided.

First, machine physical parameters have been assumed ideal in this part of evaluation, to exclude tracking error caused by parameter sensitivity. Second, the flux feedback used for the DB-DTFC algorithm is "real flux" from an ideal machine model, so that the effects from flux observer modeling can be separated. Third, a definition of flux estimation error has been given in the following as an indicator for evaluation:

$$\text{Flux Estimation Error} = \frac{\left|\left|\hat{\lambda_{qds}}\right| - \left|\lambda_{qds}\right|\right|}{\left|\lambda_{qds}\right|} \times 100\%. \quad (28)$$

Flux estimation errors are demonstrated in Fig. 5, for a wide operating range at SFs of 1.5 and 0.5 kHz, with a rated flux that is commanded. The z-axis of each plot indicates flux estimation errors generated by using either flux observers at different

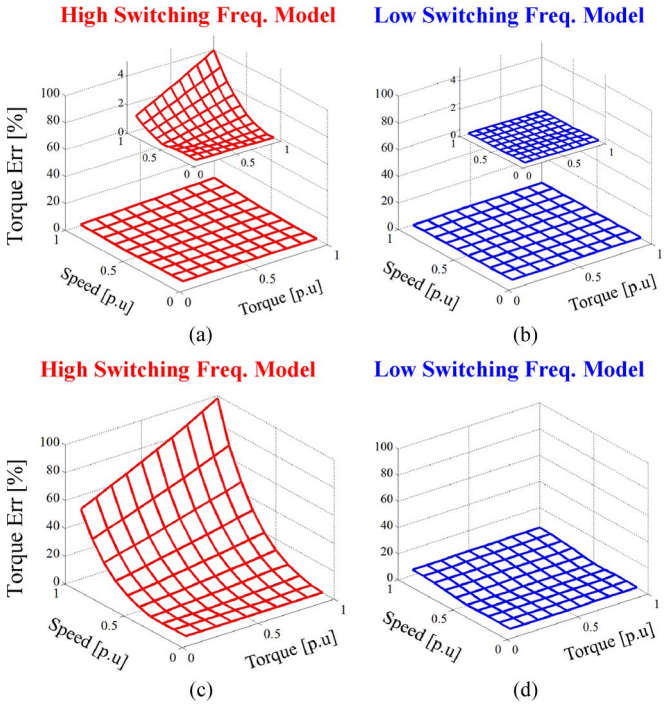

Fig. 6. Torque production errors in simulation using the high- or low-SF torque model at rated flux. (a) and (b) Switching at 1.5 kHz. (c) and (d) Switching at 0.5 kHz.

operating conditions. At both SFs, estimation errors caused by the low-SF flux observer can be reduced by upgrading to the proposed low-SF flux observer. In terms of estimation accuracy improvement, the benefits of using the low-SF flux observer are more significant at 0.5 kHz compared to the case at 1.5 kHz.

B. Torque Model Evaluation

A similar approach can be applied to evaluate the proposed low-SF Volt–second-based torque inverse model. A definition of torque production error is given in (29). To prevent unreasonable value at low torque region, rated torque is used as a base value

$$\text{Torque Error} = \frac{|T_e - T_e^*|}{T_{e_{\text{rated}}}} \times 100\%. \tag{29}$$

Torque control errors using either the high or low-SF torque inverse model are provided in Fig. 6. It is the true flux linkage, instead of estimate values, that is used for DB-DTFC control law computation. Therefore, no effect of flux observer is involved, and torque errors are entirely originated from torque inverse model. In addition, ideal machine physical parameters are used to eliminate possible errors from parameter sensitivity.

The height of surfaces in Fig. 6 indicates the torque tracking errors. At an SF of 1.5 kHz, the torque control errors by using either torque models are acceptably small, and torque accuracy is within 5% region, which is fairly acceptable. In contrast, very significant torque control errors are observed at 0.5 kHz SF with the high-SF model, particularly at high speed. By using the proposed low-SF torque model, improvements are demonstrated in Fig. 6(d).

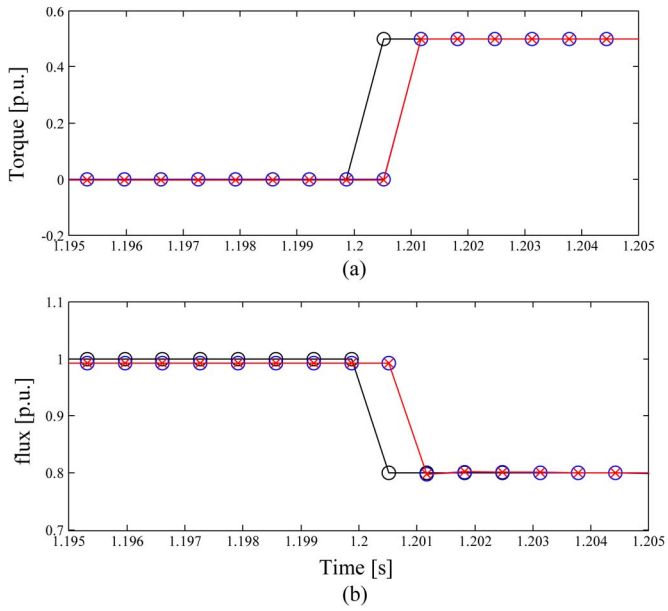

Fig. 7. Deadbeat torque and flux responses in simulation using low-SF model at rated speed and an SF of 1.5 kHz.

C. Transient Performance

Transient performance using the proposed low-SF model has also been evaluated in simulation. From Fig. 7(a) and (b), the estimated torque and flux values track the real torque and flux quantities quite precisely (nearly overlaid), with step torque and flux command at rated speed. With accurate parameters, the proposed flux observer yields torque and flux estimates that are close to the actual values, in both steady state and transients.

D. Parameter Sensitivity

For the existing DB-DTFC flux observer and torque model, the authors in [21] have provided a thorough analysis of its sensitivity to physical parameters. Key conclusions are that DB-DTFC control law demonstrates superior parameter insensitivity compared to standard IFOC drives, particularly at high-speed operation.

For the proposed low-SF DB-DTFC models, parameter sensitivity is analyzed following similar approaches used in [21]. The estimation accuracy of the proposed low-SF flux observer is shown in Fig. 8. As stated in [10] and [21], the current model is relatively sensitive to rotor resistance at high speed while the voltage model is more sensitive to stator resistance at low speed. By combining the two models with a smooth transition, the whole model demonstrates reduced sensitivity to parameters. Overall, the estimation accuracy of the proposed low-SF flux observer is comparable to the results in [10] and [21]. At low speed, the low-SF flux observer is relatively sensitive to rotor resistance and magnetizing inductance.

Parameter sensitivity evaluation on the proposed low-SF DB-DTFC torque model is provided in Fig. 9. Real flux linkage from machine model in simulation is used as feedback so that the parameter sensitivity on the flux observer has no impact on torque model evaluation. Observed from Fig. 9, the proposed

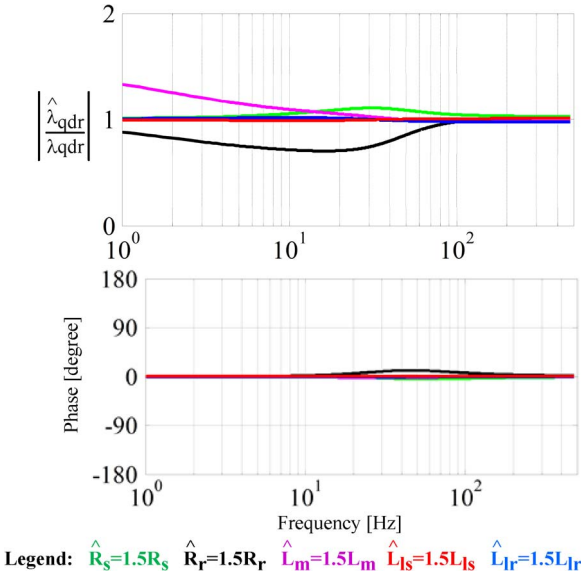

Fig. 8. Estimation accuracy of the proposed low-SF flux observer with intentionally detuned parameters, at rated slip frequency.

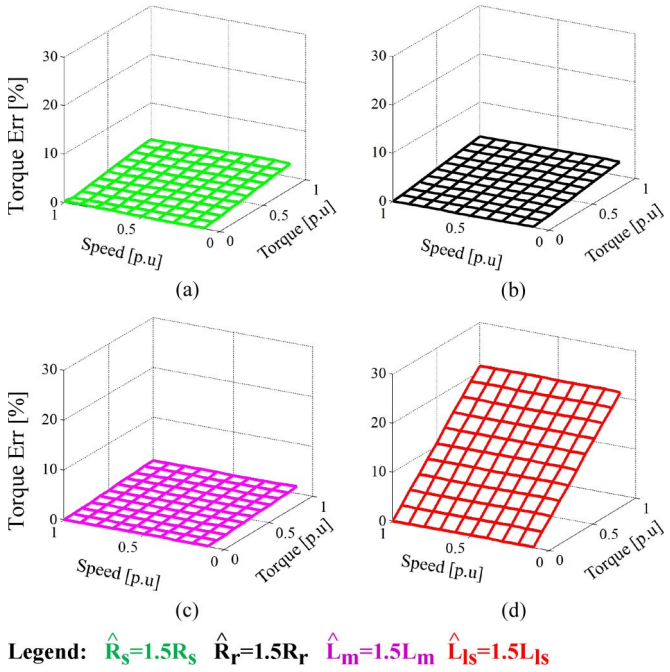

Fig. 9. Parameter sensitivity analysis of the proposed low-SF torque model with real flux as feedback. Rated flux condition. (a) 150% stator resistance. (b) 150% rotor resistance. (c) 150% magnetizing inductance. (d) 150% leakage inductance.

low-SF torque model keeps torque tracking error within 10% when stator/rotor resistance or magnetizing inductance is detuned by 50%. The most sensitive physical parameter appears to be leakage inductance.

By using the flux estimates from the low-SF model, the overall torque accuracy of the proposed DB-DTFC solution is demonstrated in Fig. 10, with the detuned parameter effects. At high speed, the system shows good parameter insensitivity to all detuned parameters, since the voltage model in the flux observer dominates and provides parameter-insensitive flux estimates. While at low speed, the detuned rotor resistance and magnetizing inductance values degrade the torque control accuracy. Since the proposed low-SF models are enhanced based on the existing DB-DTFC drives, it is not surprising to observe similar parameter sensitivity properties to the ones shown in [21].

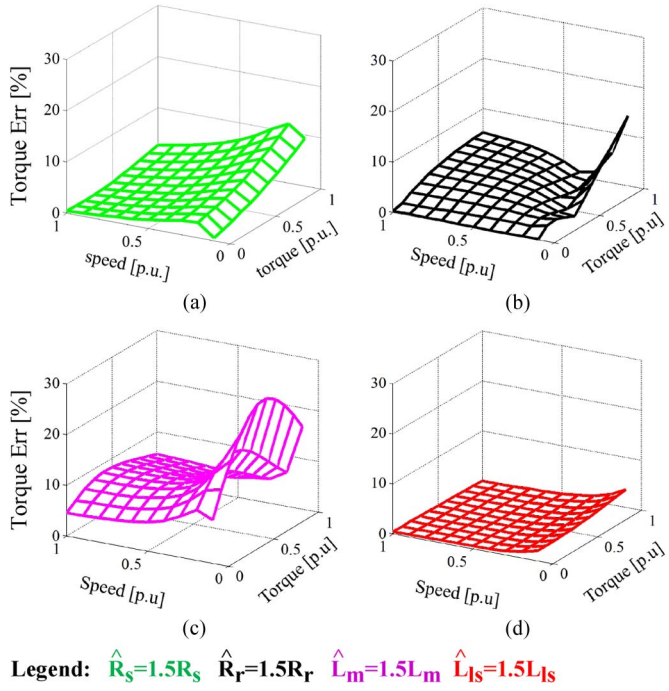

Fig. 10. Parameter sensitivity analysis of the proposed low-SF torque model with flux estimates from the proposed flux observer. Rated flux condition. (a) 150% stator resistance. (b) 150% rotor resistance. (c) 150% magnetizing inductance. (d) 150% leakage inductance.

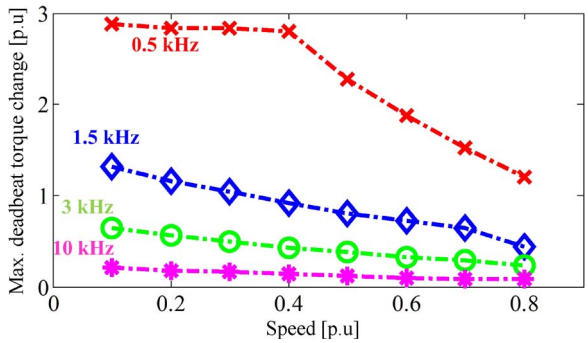

Fig. 11. Maximum deadbeat torque change at various SFs, at rated flux. DC bus voltage: 330 V.

E. Low-SF DB-DTFC Properties

Since the Volt–second vector on the inverter is the true manipulated input of DB-DTFC, the maximum Volt–second that the inverter can provide gives physical limitation of how significant torque can be changed at a particular speed. Considering the same dc bus value, the size of Volt–second hexagon is linear to its switching length. In other words, switching at lower frequencies makes it possible to have a more significant torque change over one switching period.

The maximum deadbeat torque transition at different speeds has been evaluated for various SFs and demonstrated in Fig. 11. With an increasing range of Volt–second vector provided by the

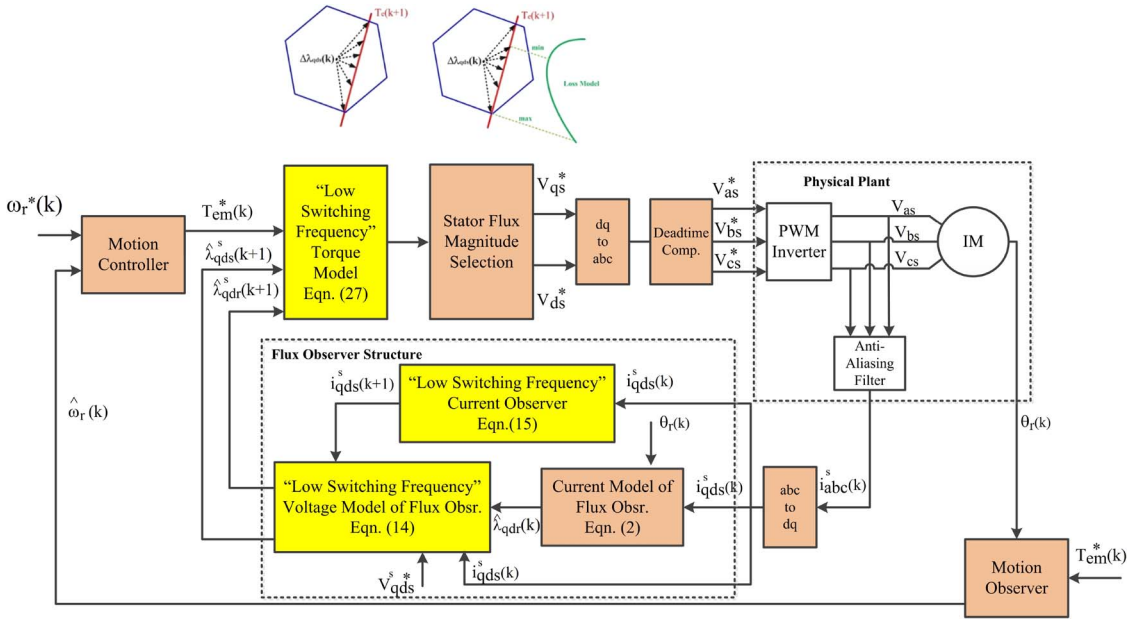

Fig. 12. Overall system block diagram of low-SF DB-DTFC.

inverter, a more significant deadbeat torque change is possible. For each particular SF, the maximum deadbeat torque change capability is generally reduced when speed is increasing, in which case higher voltages are required. At 0.5-kHz SF, the machine maximum torque is able to be achieved over one SF. With the possibility provided by low-SF DB-DTFC, it should also be noted that such significant torque change is not always favorable, particularly considering the effects on mechanical system.

V. Experimental Evaluation

A. Experimental Setup

The dynamometer setup used for experimental evaluation includes two identical 3.7-kW induction machines with rigid coupling. Physical parameters are provided in Appendix I. The machine on the motoring side is driven by DB-DTFC on a standard two-level inverter while a commercial V/F controlled drive is used to emulate the load characteristics.

An overall system diagram, including a low-SF flux observer and a low-SF torque model, is provided in Fig. 12. Blocks marked in yellow indicate the enhancement for low-SF DB-DTFC applications. Two phase currents are measured by LEM current sensors, filtered using antialiasing filters and sampled in the center of each switching period. The sampling frequency is synchronized with the SF. Nonideal effects on inverters, due to dead time and voltage drop on semiconductors, have been compensated using an experimental determined lookup table. Thus, torque and flux control errors from current measurement and/or inverter nonlinearity are not significant issues.

The symmetrical and asymmetrical PWMs provide comparable steady-state torque and flux control performance. At the torque change transient, a more accurate current estimate of the average value over the switching period can be obtained using symmetrical PWM, by sampling once at the center of the carrier waveform. The accuracy of current sampling measurement affects transient flux estimation accuracy. While the asymmetrical PWM provides faster dynamic properties, it requires more current samples in order to achieve an accurate average current estimate. For the following experimental results, symmetrical PWM voltage modulation is in use.

Torque sensor and flux sensors are not installed on the dynamometer. Real torque and flux linkage are not able to be measured and compared to their estimated values directly. However, control accuracy of torque and flux can still be indirectly evaluated. As stated before, a commercial drive is used in torque mode to emulate load properties. For accurate torque and flux control at steady-state operation, the DB-DTFC torque command, which is the output of motion controller, should be nearly same as the torque command on the load side, with consideration of mechanical damping and friction. The estimated torque should track the DB-DTFC torque command. By maintaining the same load, torque commands and torque estimates should be consistent and virtually without change, when the stator flux command is varying. In terms of transient performance, it is difficult to measure the actual torque and flux precisely in experiment. Instead, the simulation results in Fig. 7 show good tracking performance of the estimated values from observer, when ideal parameters and ideal voltage modulation are assumed.

Possible parameter errors and unmodeled dynamics including saturation effects result in torque and flux estimation and tracking inaccuracy. In addition to steady-state errors shown in Section IV-C, transient properties of torque and flux deadbeat tracking performance also degrade. However, as it is stated in [21] and discussed in the previous section, DB-DTFC is expected to be less sensitive to physical parameters than standard IFOC drive, particularly at medium and high speeds. In order to achieve a fair comparison, experimental evaluation is carried out at medium- and high-speed regions and carefully controlled from the saturation region. Moreover, it has been found in [16]–[19] and also explored in Section IV that those fast switching approximations are less accurate at high speed.

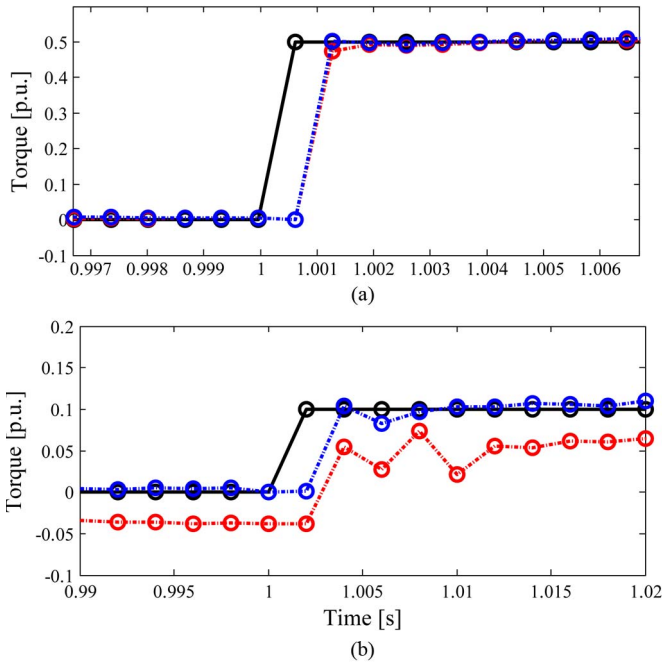

Fig. 13. Deadbeat torque responses in experiments using either the high- or low-SF model at SFs of (a) 1.5 and (b) 0.5 kHz. Operating at 0.5 per unit (p.u.) speed.

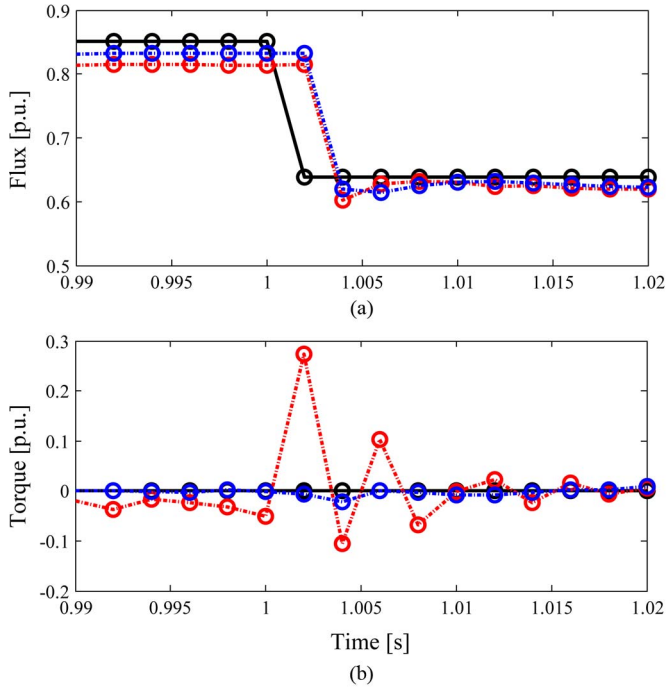

Fig. 14. Deadbeat flux responses in experiments using either high- or low-SF models at an SF of 0.5 kHz. (a) Flux response. (b) Torque response. Operating at 0.5 p.u. speed.

B. Experimental Results

A deadbeat torque response has been experimentally evaluated on the aforementioned test bench, and the results are provided in Fig. 13(a) and (b) for SFs of 1.5 and 0.5 kHz, respectively. At an SF of 1.5 kHz, both high- and low-SF models exhibit good performance. The one using low-SF models provides nearly deadbeat response while the performance of the one using the high-SF counterpart degrades at the transients but still acceptable. The existing DB-DTFC models with high-SF approximations work adequately at 1.5-kHz SF, which is also expected from the simulation results in Figs. 5 and 6. The results are not related to the magnitude of the torque command but to the SF.

For operating at lower SF such as 0.5 kHz, however, the one using high-SF flux observer and torque inverse model apparently shows poor transient dynamics as well as steady-state errors. On the other hand, the proposed low-SF model is still able to provide the desired deadbeat performance in the transients.

In addition to the deadbeat torque response, it is also known that DB-DTFC is able to achieve a deadbeat response for stator flux magnitude. More significantly, accurate and smooth air-gap torque should still be produced while stator flux magnitude varies. It can be seen in Fig. 14 that, at low SFs (e.g., 0.5 kHz), torque production is not desired when high-SF flux observer and torque inverse model are in use. The influence on torque production from flux linkages is not properly modeled. On the other hand, the torque responses with the use of low-SF models show little influence from stator flux linkage, since the cross-coupled system is recognized and properly modeled.

DB-DTFC provides intuitive graphical solutions to illustrate how the control law works. The transients shown in Fig. 14 that a step flux reference is given at time instant kT are graphically interpreted in Fig. 15, by using either the high- or the low-SF model. For Fig. 15(a), the Volt–second vector to achieve deadbeat flux response is computed based on high-SF torque inverse model, which involves the aforementioned approximations that are not acceptable at low-SF operation. As a result, the torque angle is shown at time instant $(k+1)T$, which indicates that undesired air-gap torque is produced at such no-load condition. On the other hand, Fig. 15(b) shows the results that low-SF models are in use. The Volt–second vector computed and applied at time instant kT is more accurate to achieve deadbeat flux response without affecting torque production. No torque angle appears in the flux varying transients.

VI. Scaling to High-Power Induction Machines

From the analysis and discussion in the previous sections, the performance of the low-SF DB-DTFC has been evaluated on a 3.7-kW induction machine. It is also important to investigate its potential performance on high-power rating machines, which are more likely to be operating at low SFs.

Several high-power induction machines are selected with parameters given in Appendix II. Low-SF DB-DTFC models are constructed based on the machine parameters provided. The torque tracking accuracy of each machine is evaluated in simulation, provided in Fig. 16.

The torque control errors of different machines demonstrate a similar trend over the entire operating space, when the high-SF

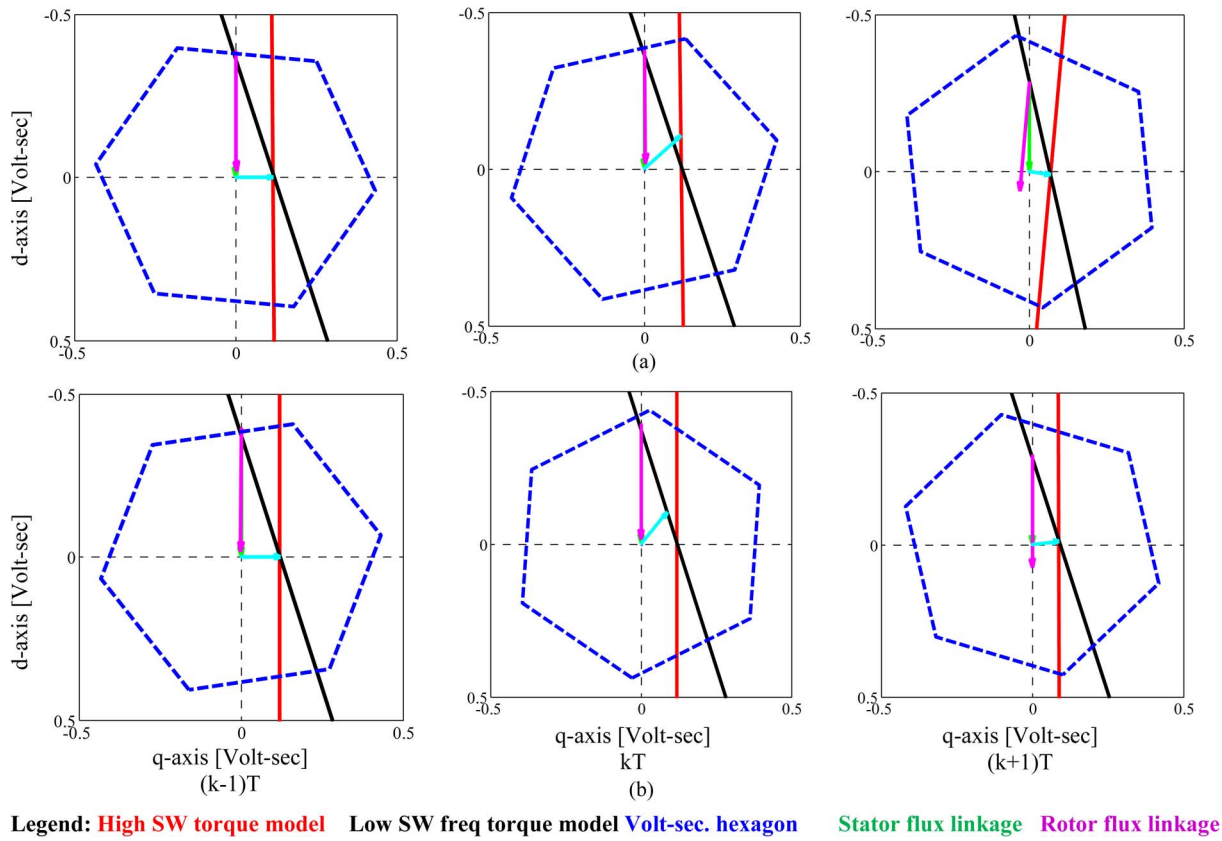

Fig. 15. Graphical solutions of deadbeat flux transients shown in Fig. 13, with either the (a) high- or (b) low-SF model in use.

models are in use. Note that the z-axis scales have been adjusted for different machines. Similar to Fig. 8, the presented torque errors can be largely reduced by using the proposed low-SF DB-DTFC model. In addition, it can be observed that the lower SF results in larger torque errors, by comparing Fig. 16(a), (b), and (d). It is reasonable to expect more improvements by using the proposed enhanced flux observer and torque model at a lower SF. Furthermore, it is shown that torque errors are increasing with the rising speed. By comparing IM2 and IM3 operating at the same SF, more torque errors are shown in Fig. 16(c) at rated operating conditions because the rated speed is higher.

Relationships between torque errors and SFs are provided in Fig. 17, where an SF range from 0.5 to 3 kHz is covered by using either the high- or low-SF models. It is noted that the effects from SF is highly nonlinear. For all induction machines under evaluations, the DB-DTFC torque control errors using the high-SF model increase significantly when the SF is reduced to 1 kHz or even lower, shown in Fig. 17(a). The proposed low-SF model is preferred for torque accuracy improvements, which reduces errors to an acceptable level, shown in Fig. 17(b).

Based on the comparison of torque tracking errors provided in Fig. 17, it is safe to conclude that, at an SF lower than 1 kHz, the proposed low-SF models should be used to keep torque errors within an acceptable range. For an SF higher than 1.5 kHz, torque estimation and tracking error is not significant even using the existing high-SF DB-DTFC models. In order to reduce computation efforts, the existing models with high-SF approximations are acceptable.

The proposed low-SF DB-DTFC model should be applicable for any SFs for which the coefficients are calculated for. However, a couple of issues may limit its performance when SF is further reduced. First, SF should be sufficiently high compared with machine fundamental frequency, to provide acceptable voltage modulation and harmonic content. Second, as stated in modeling process in Sections II and III, the assumption that shaft speed change is negligible over switching period should be satisfied to maintain good performance of the low-SF DB-DTFC. It is suggested that an SF at least ten times higher than the machine fundamental frequency should be in use.

From the simulation results in Figs. 16 and 17, the proposed low-SF models provide DB-DTFC solutions that are possible to be implemented on high-power induction machines at very low SFs. Further challenges to integrate DB-DTFC on large machines and achieve nearly ideal performance are associated with inverter voltage modulation, which is beyond the scope of this paper. Ongoing research to include voltage modulation for large machines will be a significant focus for future publications.

VII. Conclusion

The key conclusions for this paper are summarized as follows.

1) The existing flux observer models work adequately at high SFs, but the fast switching approximations embedded are less accurate at low SFs, which lead to flux estimation errors.

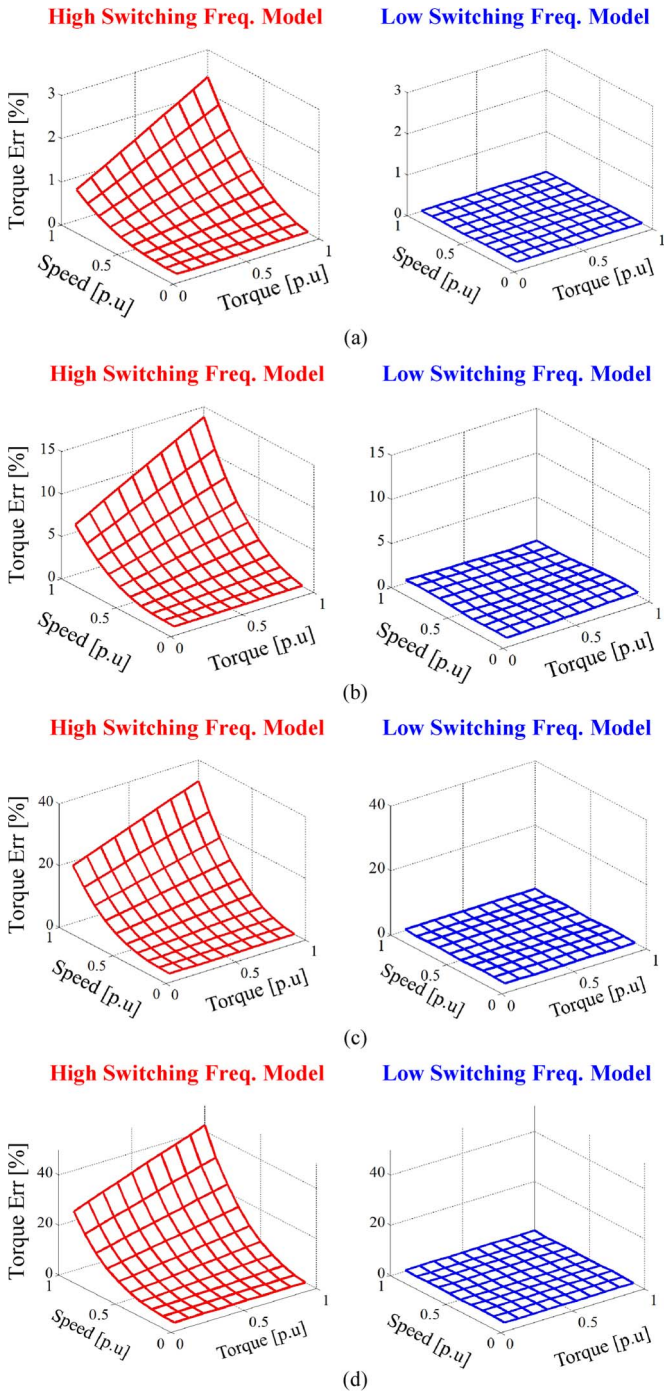

Fig. 16. Torque production error evaluation in simulation for high-power rating induction machines listed in Appendix II, with rated flux at their used SFs. (a) IM1 at 1.6 kHz. (b) IM2 at 0.8 kHz. (c) IM3 at 0.8 kHz. (d) IM4 at 0.5 kHz.

2) The proposed low-SF flux observer can be developed by cross-solving the coupled stator flux linkage and stator current differential equations in the discrete-time domain. Flux estimation accuracy has been improved particularly at low SFs.
3) The original Volt–second-based inverse torque model performs well at high SFs. At low SFs, the torque derivative is poorly approximated as the average rate of change of torque over one switching period, which induces torque production errors.

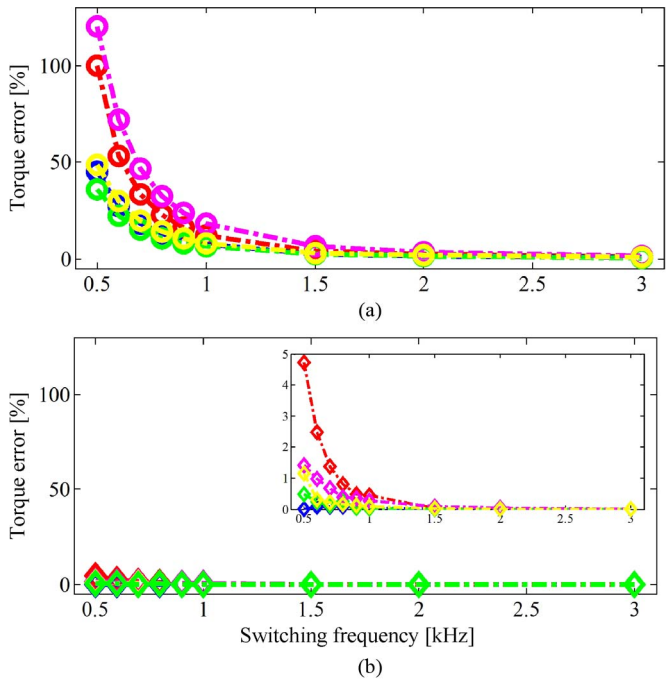

Legend: Test motor **(Appendix I),** IM1, IM2, IM3, IM4 **(Appendix II)**

Fig. 17. Torque production errors at different SFs for induction machines at rated operating conditions. (a) Using the high-SF models. (b) Using the low-SF models.

TABLE I
TEST INDUCTION MACHINE PARAMETERS

Power rating	3.7[kW]
Rated speed	855[min^{-1}]
Poles	8
Stator resistance	0.3960[Ω]
Rotor resistance	0.4010[Ω]
Magnetizing inductance	29.4[mH]
Stator leakage inductance	2.1[mH]
Rotor leakage inductance	2.5[mH]

TABLE II
HIGH-POWER INDUCTION MACHINE PARAMETERS

Induction Machines	Power Ratings [kW]	Switching Frequency [kHz]	Rated sync. Frequency [Hz]	Rated Torque [kN-m]
IM1	800	1.6	49	4.68
IM2	750	0.8	51	7.79
IM3	4800	0.8	70.4	10.85
IM4	1700	0.5	50.5	10.71

4) The proposed low-SF torque model can be integrated with DB-DTFC, which minimizes the torque errors and promotes drive performance with very little SF dependence.
5) The proposed low-SF flux observer and low-SF torque model are also feasible to be integrated on high-power induction machines.

APPENDIX I

See Table I.

APPENDIX II

See Table II.

REFERENCES

[1] R. Lorenz, "The emerging role of deadbeat, direct torque & flux control in the future of induction machine," in *Proc. Optim. Elect. Electron. Equipment Conf.*, 2008, pp. 19–27.

[2] B. Kenny and R. Lorenz, "Stator and rotor flux based deadbeat direct torque control of an induction machine," *IEEE Trans. Ind. Appl.*, vol. 39, no. 4, pp. 1093–1101, Jul./Aug. 2003.

[3] T. Obermann, Z. Hurst, B. Bradley, and R. Lorenz, "Deadbeat–direct torque & flux control motor drive using a single control law to minimize motor losses," in *Proc. Int. Elect. Mach. Syst. Conf.*, Oct. 2010, pp. 742–747.

[4] T. Habetler, F. Profumo, M. Pastorelli, and L. Tolbert, "Direct torque control of induction machines using space vector modulation," *IEEE Trans. Ind. Appl.*, vol. 28, no. 5, pp. 1045–1053, Sep./Oct. 1992.

[5] T. Habetler, F. Profumo, G. Griva, M. Pastorelli, and A. Bettini, "Stator resistance tuning in a stator-flux field-oriented drive using an instantaneous hybrid flux estimator," *IEEE Trans. Power Electron.*, vol. 13, no. 1, pp. 125–133, Jan. 1998.

[6] D. Novotny and T. Lipo, *Vector Control and Dynamic of AC Drives*. New York, NY, USA: Oxford Univ. Press, 1996.

[7] M. Depenbrock, "Direct self-control (DSC) of inverter-fed induction machine," *IEEE Trans. Power Electron.*, vol. 3, no. 4, pp. 420–429, Oct. 1988.

[8] I. Takahashi and T. Noguchi, "A new quick-response and high efficiency control strategy of an induction motor," *IEEE Trans. Ind. Appl.*, vol. 22, no. 5, pp. 820–827, Sep./Oct. 1986.

[9] P. Jansen and R. Lorenz, "A physically insightful approach to the design and accuracy assessment of flux observers for field oriented induction machine drives," *IEEE Trans. Ind. Appl.*, vol. 30, no. 1, pp. 101–110, Jan./Feb. 1994.

[10] N. West and R. Lorenz, "Digital implementation of both a stator and rotor flux linkage observer and stator current observer for direct torque and flux control of induction machines," *IEEE Trans. Ind. Appl.*, vol. 45, no. 2, pp. 729–736, Mar./Apr. 2009.

[11] G. Vershese and S. Sanders, "Observers for flux estimation in induction machines," *IEEE Trans. Ind. Electron.*, vol. 35, no. 1, pp. 85–94, Feb. 1988.

[12] R. Nilsen and M. Kazmierkowski, "New reduced-order observer with parameter adaptation for flux estimation in induction motors," *Proc. IEEE Power Electron. Spec. Conf.*, vol. 1, pp. 242–252.

[13] T. Orlowska-Kowalsa, "Application of extended Luenberger observer for flux and rotor time-constant estimation in induction motor drive," *IEE Proc. D, Control Theory Appl.*, vol. 136, no. 6, pp. 323–339, Nov. 1989.

[14] H. Rehman, A. Deriyok, M. Guven, and L. Xu, "A new current model flux observer for wide speed range sensorless control of an induction machine," *IEEE Trans. Power. Electron.*, vol. 17, no. 6, pp. 1041–1048, Nov. 2002.

[15] L. Harnefors, "Design and analysis of general rotor flux oriented vector control system," *IEEE Trans. Ind. Electron.*, vol. 48, no. 2, pp. 383–389, Apr. 2001.

[16] C. Bottura, J. Silvino, and P. Resende, "A flux observer for induction machine base on a time-variant discrete model," *IEEE Trans. Ind. Appl.*, vol. 29, no. 2, pp. 349–354, Mar./Apr. 1993.

[17] C. Zell and A. Medvedev, "Sampled-data flux estimation in induction machines," in *Proc. IEEE Int. Conf. Control Appl.*, 1996, pp. 1102–1107.

[18] R. Bojoi, G. Griva, and F. Profumo, "Field oriented control of dual three-phase induction motor drives using a Luenberger flux observer," in *Conf. Rec. IEEE IAS Annu. Meeting*, Oct. 2006, pp. 1253–1260.

[19] L. Diao, D. Sun, K. Dong, L. Zhao, and Z. Liu, "Optimized design of discrete traction induction motor model at low switching frequency," *IEEE Trans. Power Electron.*, vol. 28, no. 10, pp. 4803–4810, Oct. 2013.

[20] W. Xu and R. Lorenz, "Dynamic loss minimization using improved deadbeat–direct torque and flux control for interior permanent magnet synchronous machines," *IEEE Trans Ind. Appl.*, vol. 50, no. 2, pp. 1053–1065, Mar./Apr. 2014.

[21] B. Heinbokel and R. Lorenz, "Robustness evaluation of deadbeat, direct torque and flux control for induction machine drives," in *Proc. 13th Eur. Conf. EPE*, Sep. 2009, pp. 1–10.

Yukai Wang (S'13) was born in Ningbo, China. He received the B.S. degree in electrical engineering from Tianjin University, Tianjin, China, in 2011 and the M.S. degree in mechanical engineering from the University of Wisconsin–Madison, Madison, WI, USA, in 2013, where he is currently working toward the Ph.D. degree.

His research interests include electrical machines and drive control technology.

Shunsuke Tobayashi received the B.S. and M.S. degrees in electrical and electronic engineering from Chiba University, Chiba, Japan, in 2008 and 2010, respectively.

Since April 2010, he has been with Toshiba Mitsubishi–Electric Industrial Systems Corporation, Fuchu, Japan. From August 2012 to February 2013, he was a Visiting Researcher at the University of Wisconsin–Madison, Madison, WI, USA. He currently develops motor drive inverters, particularly medium-voltage class for industrial applications.

Robert D. Lorenz (S'83–M'84–SM'91–F'98) received the B.S., M.S., and Ph.D. degrees from the University of Wisconsin–Madison, Madison, WI, USA, and the M.B.A. degree from the University of Rochester, Rochester, NY, USA.

Since 1984, he has been a member of the faculty of the University of Wisconsin–Madison, where he is the Mead Witter Foundation Consolidated Papers Professor of Controls Engineering in the Department of Mechanical Engineering and is the Codirector of the Wisconsin Electric Machines and Power Electronics Consortium. Prior to joining the university, he worked 12 years in industry, in Rochester, NY, USA, on high-performance drives and synchronized motion control. He has authored over 300 published technical papers and is the holder of 24 patents with nine more pending.

Dr. Lorenz was the IEEE Division II Director for 2005/2006, the IEEE Industry Applications Society (IAS) President for 2001, and a Distinguished Lecturer of the IEEE IAS for 2000/2001. He received the 2003 IEEE IAS Outstanding Achievement Award, the 2006 EPE PEMC Outstanding Achievement Award, the 2011 IEEE IAS Distinguished Service Award, the 2014 IEEE Richard H. Kaufman Technical Field Award, and the 2014 EPE Outstanding Achievement Award. He has won 32 IEEE prize paper awards on power electronics, drives, self-sensing, current regulators, motion control, etc.